Spatial and temporal variability of oceanic heat flux to the Arctic ice pack

Richard A. Krishfield

Woods Hole Oceanographic Institution, Woods Hole, Massachusetts, USA

Donald K. Perovich

Cold Regions Research and Engineering Laboratory, Hanover, New Hampshire, USA

[1]   In order to simulate the large-scale structure and temporal variability of oceanic heat flux (F_w) to the Arctic perennial ice pack, observations of heat in the mixed layer and ice dynamics are compared with parameterizations and climatologies. Long-term drifting platform observations of seawater temperature and salinity (primarily from automated buoys) are used to describe the annual cycle of temperature above freezing (ΔT_f) in the mixed layer beneath the ice pack, which are modulated by ice-ocean friction velocities ($u*$) determined from the platform drifts to produce estimates of F_w between 1975 and 1998. On average, ΔT_f is not negligible in winter, especially in the Transpolar Drift, which implies a positive F_w to the ice pack by means other than solar heating. A parameterization based solely on the solar zenith angle (with a 1 month lag) is found to largely describe the observed ΔT_f (with root mean square error of 0.03°C), despite the lack of an albedo or open water term. A reconstruction of F_w from 1979 to 2002 is produced by modulating parameterized ΔT_f with $u*$ on the basis of daily ice drift estimates from a composite satellite and in situ data set. The reconstructed estimates are corrected for regional variations and are compared to independent estimates of F_w from ice mass balance measurements, indicating annual F_w averages between 3 and 4 W m^{-2} depending on the selection of under-ice roughness length in the ice-ocean stress calculations. Although the interannual variations in ΔT_f are fixed by the parameterization in the derived reconstruction, the dynamics indicate an overall positive trend (0.2 W m^{-2} decade^{-1}) in Arctic F_w, with the largest variations found in the southern Beaufort Gyre.

1.   Introduction

[2]   The equilibrium thickness of the pack ice in the central Arctic is believed to be sensitive to changes in the oceanic heat flux (F_w) from the seawater to the ice [*Maykut and Untersteiner*, 1971]. The product of heat and turbulence at the ice-ocean interface, F_w is a poorly understood component of recent global climate change studies. Most of the heat that is transmitted to the underside of the ice pack is suspected to be from solar radiation rather than from upwelling warmer water [*Maykut*, 1982; *Maykut and Perovich*, 1987], but storm-induced instances of upwelling and entrainment of warmer deeper water have been reported [*Yang et al.*, 2001]. Models suggest that the equilibrium ice thickness of 3 m may be maintained by an annual average bottom heat flux of 2 W m^{-2} [*Maykut*, 1982], but observations usually exceed that value. Typical estimates for the central Arctic are 4 W m^{-2} (or more) from June through August and 0 W m^{-2} for the remainder of the year [*Maykut*

and McPhee, 1995], however, the observations are sparse in space and time, which hampers confident basin-wide estimates. The seasonality of the heat and salt budgets between the ice pack and upper ocean, and the significance of transient effects on these balances, are important concerns for understanding changing Arctic sea ice mass balance and changes in upper ocean properties. Since evidence suggests that the ice extent and thickness are decreasing in the Arctic [*Comiso*, 2002; *Rothrock et al.*, 2003], a better knowledge of the contribution of F_w is needed.

[3]   Direct turbulence measurements of F_w are difficult to make, since they require frequent, high precision determinations of temperature, salinity, and vertical velocity in the near-surface boundary layer under drifting sea ice [e.g., *McPhee and Stanton*, 1996]. The turbulent fluxes are computed using a Reynolds analogy to estimate ensemble means from covariances. As a result, direct measurements of F_w are sparse in space and time. On the basis of direct measurements from 3 ice camps, a simplified parameterization [*McPhee*, 1992] was developed to estimate F_w by modulating the mixed layer temperature above freezing (ΔT_f) by the ice-ocean friction velocity ($u*$), where $u*$ is

Table 1. Duration and Dates of Observations

Platform	Observations[a]	Start	Day	End	Day
	Beaufort Gyre Time Series				
AIDJ_BB	211	Apr-75	102	Oct-75	274
AIDJ_BF	307	May-75	132	Apr-76	112
AIDJ_CB	408	May-75	135	Apr-76	117
AIDJ_SB	296	May-75	138	Apr-76	112
SAL_947	168	Apr-85	106	Oct-85	304
SAL_895	347	Apr-86	94	May-87	121
SAL_896	101	Sep-86	268	Jan-87	28
SAL_897	238	Sep-86	257	Jul-87	182
SAL_289[b]	206	May-88	131	Nov-88	335
SAL_369	39	Mar-90	83	Apr-90	120
SAL_790	381	Apr-92	107	Apr-93	120
SAL_797	120	Sep-93	247	Dec-93	365
SAL_795	129	Oct-93	297	Mar-94	60
B96IOEB	338	May-96	122	Apr-97	98
B97IOEB	264	Apr-97	102	Dec-97	365
SHEBA	327	Oct-97	291	Sep-98	273
Total	3880				
	Transpolar Drift Time Series				
FRAM_1	87	Mar-79	90	May-79	126
SAL_283	245	May-88	123	Dec-88	366
SAL_285	280	May-88	147	Feb-89	59
SAL_288	828	May-88	143	Aug-90	213
SAL_286	30	Jun-88	154	Jul-88	183
CEAREXO	29	Mar-89	89	Apr-89	118
SAL_103	396	Sep-90	270	Nov-91	299
SAL_104	342	Sep-90	268	Aug-91	243
SAL_108	39	Sep-90	267	Oct-90	304
SAL_792	48	Mar-91	74	Apr-91	120
SAL_793	46	Apr-92	108	May-92	152
SAL_794	199	Apr-92	108	Oct-92	305
SAL_798	181	Sep-93	245	Feb-94	59
T94IOEB	107	Apr-94	103	Jul-94	210
SAL_798	159	May-94	147	Nov-94	305
Total	3016				
	Other				
SAL_284	685	Apr-90	107	Feb-92	60

[a]Daily (buoy) or semidaily (ice camp) averages.
[b]Removed for anomalous high F_w along slope.

determined from a statistical relationship based on ice drift velocity. Another indirect method estimates time-averaged F_w from ice thermistor profiles [*McPhee and Untersteiner*, 1982; *Perovich et al.*, 1989].

[4] In this investigation, F_w is estimated using the *McPhee* [1992] equations on 32 long-term drifting platforms between 1975 and 1998, including over 7500 observation days. The observations of heat in the Arctic mixed layer and ice dynamics are compared with a hydrographic climatology and satellite sea ice motion data set. The hydrographic climatology inadequately depicts the annual cycle of ΔT_f, so a parameterization based on the solar zenith angle and day of the year is introduced. A reconstruction of F_w from 1979 to 2002 is produced by using the *McPhee* [1992] equations to modulate the parameterized ΔT_f with u^* derived from the daily ice motion data set. The reconstruction is corrected for regional variations, and compared to independent estimates of F_w from ice mass balance measurements in order to provide a better understanding of the basin-scale character of F_w beneath the perennial pack ice, and to analyze the annual and interannual variability due to the dynamics of the ice motion.

[5] In section 2, the observations and climatological data are described. The methods of calculating the quantities of

interest are given in section 3. Estimates from the observations and reconstruction, factors influencing accuracy, and decadal and interannual variability are presented in section 4. Section 5 discusses the results.

2. Data

2.1. Observations

[6] The primary hydrographic data analyzed here are Lagrangian time series of measurements at 8 or 10 m depths from 21 SALARGOS buoys and 2 Ice-Ocean Environmental Buoys (IOEBs) that were deployed between 1985 and 1998 at various locations across the Arctic. Usually between 1 and 5 buoys were deployed at any time. These are augmented with historical STD or CTD data from the AIDJEX, FRAM, CEAREX, and SHEBA ice camps (Table 1). Since all of these platforms are fixed to the floating icepack, ice drift vectors may be computed from location time series (Figure 1). The drift pattern of ice floes (and buoys) generally fall into two categories: west (Canada basins) or east (Eurasian basins) Arctic. The west is characterized by the Beaufort Gyre surface anticyclonic circulation and near surface salinity minimum, while the east is characterized by the surface Transpolar Drift that exports sea ice through the Fram Strait.

[7] SALARGOS (or Polar Ocean Profiler; POP) buoys are ice-tethered drifters with Argos location, air temperature and pressure, and six SeaBird temperature and conductivity sensor pairs suspended beneath the ice to as much as 300 m [*Morison et al.*, 1982]. The basic configuration of the SALARGOS and POP buoys was the same, except that the SALARGOS buoys of the 1980s used SBE-3 and SBE-4 sensors, while the POP buoys of the 1990s used SBE-16 sensors and included pressure sensors at more depths. Both systems are referred to as SALARGOS buoys in this paper. The data utilized here are from the uppermost seawater measurement at 10 m, which is usually located in the surface mixed layer below local surface disturbances. Twenty-four SALARGOS buoys were deployed throughout the Arctic between 1985 and 1996 by the Polar Science Center, University of Washington. The lifetime of the expendable systems varied from as little as 1 month to over 2 years. These data were contributed to the Joint Russian-American Environmental Working Group Arctic Atlas CD-ROMs (EWG, available at http://www.nsidc. colorado.edu/data/ewg/), and are provided on the International Arctic Buoy Program (IABP, available at http://iabp. apl.washington.edu) CD-ROM (version 1.0) in 12 minute and 10 day averages. The accuracy of the SeaBird sensors are expected to be about ±0.01°C and ±0.05 PSU, but without postdeployment calibrations, it is impossible to precisely determine sensor drifts. However, obvious malfunctions and a few spurious Argos locations were removed, resulting in 5207 days of temperature and salinity observations at 10 m from 21 SALARGOS buoys.

[8] The IOEB system consists of a surface flotation package which supports the meteorological and ice sensors, and houses data loggers, transmitters, antennae, and batteries [*Krishfield et al.*, 1993; *Honjo et al.*, 1995; *Krishfield et al.*, 1999]. Suspended from the surface float is a 110 m long mooring system that includes precision salinity and temperature recorders, current profiling, and biogeochemi-
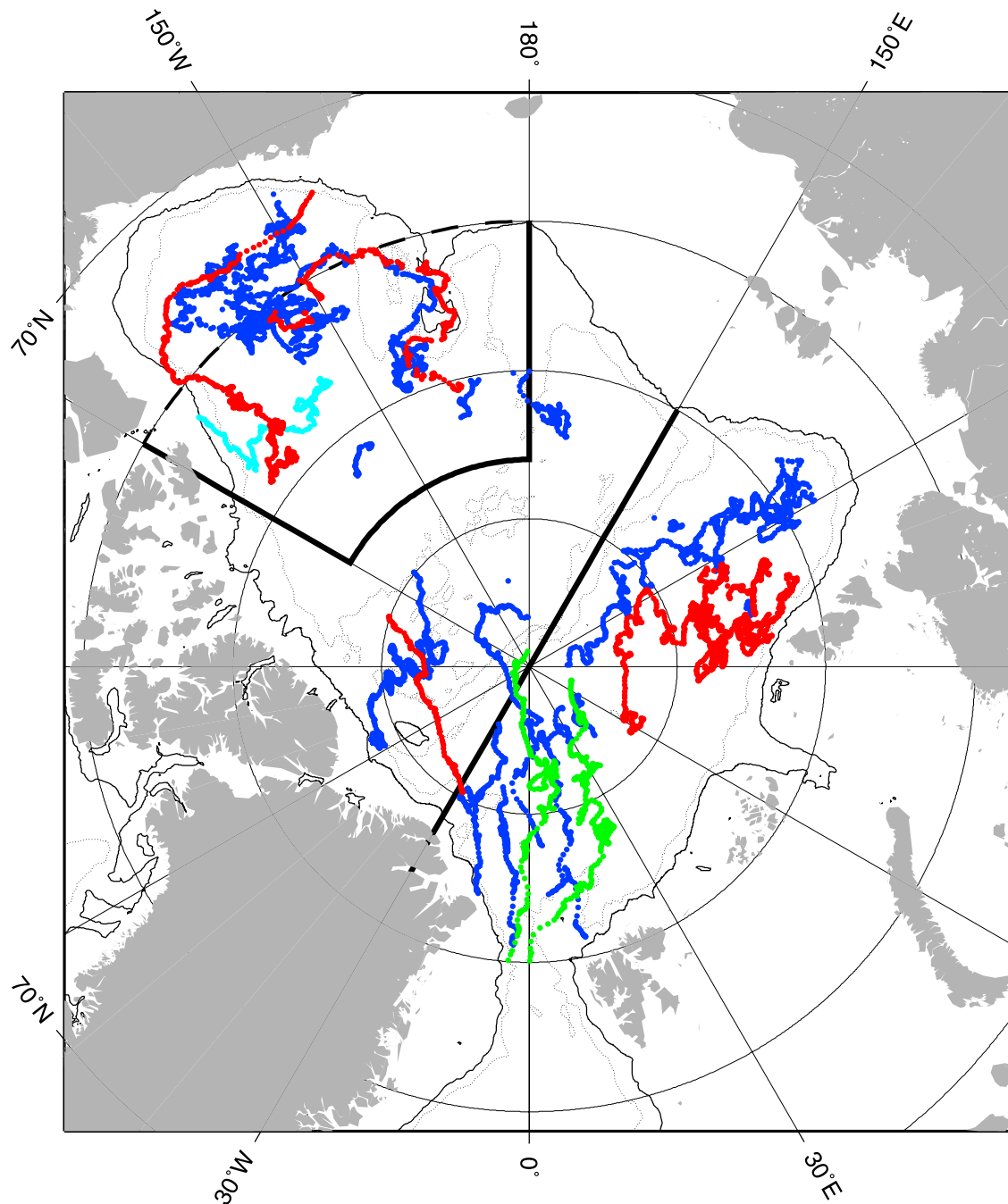
Figure 1. Drift tracks of all platforms used in this study. Those selected for Figure 6 are indicated in red. The buoy indicated in cyan was removed from the calculations for anomalous data near the slope. The drift tracks of the measurements from the ice mass balance and JCAD buoys are plotted in green. The thick solid lines delineate the upper boundaries of the Beaufort Gyre (top left, between 120°W–180° and south of 83°N) and Transpolar Drift (bottom right, between 30°W and 150°W) regions. The southern boundaries are defined by the 50% ice contour from satellite data (which vary depending on month and year) or 500 m isobath (thin solid line).

cal sensors. In April 1996, an IOEB in the Beaufort Gyre was recovered after 4 years of drift since being deployed at the LEADEX ice camp. Sensors and batteries were replaced, and the system was redeployed on a similar nearby ice floe within one week (B96IOEB). In April 1997, the system was again visited, the sensors and batteries were replaced, and the package was redeployed (B97IOEB).

Although this IOEB was subsequently never recovered, over 2 years of near-continuous data from the air, ice, and upper ocean sensors were made available via Argos satellite transmission before the system drifted onto the Chukchi shelf. Another IOEB was deployed north of Fram Strait in the Transpolar Drift (T94IOEB), and drifted for 9 months before being recovered east of Greenland.

[9] SeaBird SBE-16 SeaCats are used at three locations (8, 43 and 75 m) along the IOEB mooring for salinity and temperature measurements. Data from the instrument at 8 m on both IOEBs described above are presented. The temperature measurements are accurate to ±0.01°C and the salinity to ±0.05 PSU, although minor uncertainties exist in the depth determinations because of mooring declination. Calibrations were performed before being deployed in 1996 and in 1997, and indicate that sensor drifts for the moored instruments are within the stated accuracies (temperature < 0.005°C yr^{-1}, salinity < 0.002 month^{-1}). Because the IOEB redeployed in 1997 was not recovered, no postcalibration of the 1997–1998 SeaCat data was performed. However, there were no obvious shifts indicated in the data that were telemetered. IOEB data are available at http://ioeb. whoi.edu/.

[10] Although ice camp hydrographic measurements have historically been acquired less frequently than these buoy data, they do provide additional time series of mixed layer properties and ice drift, and sometimes other independent heat flux observations. Semidaily STD data from the four AIDJEX ice camps in the Beaufort Sea were obtained from the National Snow and Ice Data Center (NSIDC, available at http://www.nsidc.colorado.edu/), spanning the period April 1975 to April 1976 [Bauer et al., 1980; Maykut and McPhee, 1995]. The accuracy of these earlier STD data is reported to be ±0.03 in both temperature and salinity [Bauer et al., 1980; Maykut and McPhee, 1995], so is less precise than the buoy data. Also available from the NSIDC, the CEAREX CD-ROM (available at http://www.nsidc. colorado.edu/data/nsidc-0020.html) provides CTD data in the Transpolar Drift from the CEAREX oceanography camp in spring 1989, as well as STD data from the spring Fram 1979 and 1981 ice camps. From October 1997 to September 1998, the SHEBA ice camp employed a yo-yo CTD down to 150 m depth, and these data were obtained from the UCAR/NOAA CODIAC website via the SHEBA homepage (http://sheba.apl.washington.edu/). The accuracy of the data from the post-AIDJEX ice camps is believed to be the same quality as the buoy data.

[11] The aforementioned time series compose the main observational data set. An independent means of calculating F_w utilizes time series of ice thermistor profiles. Over the past decade nearly year-long drifting ice temperature profile time series were acquired by several automated ice mass balance buoys [Perovich et al., 1997, 2003] and on the IOEBs. The ice thermistor strings provide temperature readings with an accuracy of about 0.1°C from above the surface of the ice to beneath the bottom surface, with vertical spacings as tight as 5 cm between sensors located around the ice bottom (which limits the resolution in ice bottom determinations). Acoustic sensors are used on the newer ice mass balance buoys to measure the position of the ice bottom to 1 cm.

[12] Estimates of F_w from the ice data are compared to estimates of F_w using coincident hydrographic data obtained from the IOEBs or JAMSTEC Compact Arctic Drifters (JCAD, available at http://www.jamstec.go.jp/arctic/ J-CAD_e/jcadindex_e.htm). Similar to the IOEB, the JCAD also obtains hydrographic time series at discrete depths, but use SeaBird Microcats and the uppermost JCAD measurement is located at 25 m below the surface (instead of at 10 m

as the IOEB). The 25 m data from two JCADs that were deployed at the North Pole in spring 2000 and 2002 [Kikuchi and Hosono, 2003] are also used to compute F_w, by assuming that the surface layer is truly mixed to at least 25 m and substituting those observations at 10 m.

2.2. Climatological Data

[13] For comparison with the observations, and to provide similar information on broader temporal and spatial scales across the entire Arctic basin, a hydrographic climatology and ice drift data set are employed. Mean monthly temperature and salinity information at 1° grid spacing and standard depths were obtained from the Polar Hydrographic Climatology, version 2.1 (PHC; http://psc.apl.washington. edu/Climatology.html) [Steele et al., 2001]. The PHC is a merged data set combining the accuracy but low temporal resolution of the EWG at high latitudes (only two climatological seasons) with the relatively data-poor (without the historical Russian data) but higher temporal resolution of the World Ocean Atlas (WOA; http://www.nodc.noaa.gov/). However, (1) the annual cycle is not derived from monthly mean data, but instead from winter and summer endpoints by applying an arbitrary cyclic function, and (2) there is a discontinuity between 82.5 and 83°N where the EWG and WOA are merged (which has since been corrected in PHC version 2.2). For the purposes of this study, mixed layer properties are characterized by the temperature and salinity values at 10 m. Since the PHC climatology is described for only one annual cycle, interannual or decadal variations in thermal and freshwater budgets are neglected.

[14] Daily sea ice motion vector grids from 1979 through 2003 [Fowler, 2003] were obtained from the NSIDC (available at http://www.nsidc.colorado.edu/data/nsidc-0116.html). Vectors are computed from Advanced Very High Resolution Radiometer (AVHRR), Scanning Multichannel Microwave Radiometer (SMMR), Special Sensor Microwave/Imager (SSM/I), and IABP buoy data, combined using optimal interpolation, and reprojected to 25-km EASE-Grids. In order to estimate the accuracy of the gridded data set, Fowler interpolated several years of vectors to the same grid but without using the buoy data, and determined that the mean differences for each vector component was less than 0.5 cm s^{-1}, with root mean square error of approximately 3 cm s^{-1}. However, surface melt ponds on the ice and increased cloud cover in summer reduces the number and location of vectors that can be determined from the satellite data so that individual summer daily ice motion grids may contain significant noise.

3. Methods

3.1. Turbulent F_w Calculations

[15] Using the mixed layer temperature and salinity, and ice drift data previously described, the quantities that are evaluated are seawater density (σ), ΔT_f, u^*, and F_w. The freezing point of seawater and σ are calculated from the seawater temperature, salinity, and pressure (converted from depth) using the CSIRO toolkit (ftp://ftp.marine.csiro.au/ pub/morgan/seawater/) on the basis of UNESCO 1983 equations [Fofonoff and Millard, 1983]. ΔT_f is merely the difference of the temperature from the freezing point tem-

perature. Either adding heat or removing fresh water will elevate ΔT_f in seawater of fixed pressure and volume.

[16] A statistical relationship [McPhee, 1979] is used throughout the present study to determine $u*$ from the square root of the kinematic ice-ocean stress (τ):

$$u* = \sqrt{\tau} \qquad (1)$$

where

$$\tau = 0.0104 * V^{1.78} \qquad (2)$$

and V is the difference of the ice velocity from the surface geostrophic current velocity.

[17] In the same study [McPhee, 1979], a steady state planetary boundary layer model was also adapted to describe the relationship. Inherent in the model are Rossby similarity constants, and the undersurface roughness (z_0), which were fixed on the basis of AIDJEX measurements. Recent results from the SHEBA ice camp [McPhee, 2002] suggest that z_0 for undeformed multiyear ice is more than an order of magnitude less than the AIDJEX estimates, which would reduce the calculated $u*$ considerably. Therefore there is an arbitrary systematic error associated with specifying z_0 (which is considered in the discussion section). Furthermore, tides and the geostrophic current in the Arctic are relatively small in the Arctic ice pack (typically less than 5 cm s^{-1}, with the exception of local submesocale eddies in the halocline), are neglected here when evaluating τ, so are another potential source of error (a difference of 5 cm s^{-1} in V produces a difference in computed F_w of less than 5 W m^{-2} for ΔT_f less than 0.05°C).

[18] Using the McPhee [1992] equations, F_w is estimated by modulating the mixed layer ΔT_f by $u*$ according to

$$F_w = \rho c_p c_h u* \Delta T_f \qquad (3)$$

where ρ is seawater density (= $1000 + \sigma$), c_p is specific heat of seawater near freezing (= 3980 J kg^{-1}), and c_h is the heat transfer coefficient (= 0.006).

3.2. F_w From Ice Temperature Profiles

[19] McPhee and Untersteiner [1982] described how the average F_w in ice covered regions can be calculated from ice growth, temperature and salinity profiles. The conductive, specific, and latent fluxes of the lower portion of the ice floe are determined from the ice profiles, and F_w is the residual in the heat balance. The conductive heat component can be estimated fairly accurately from the temperature profiles, and careful selection of the reference layer in thick floes can keep the specific heat storage component small in the calculations. Consequently, the source of the greatest error in the heat balance is typically associated with resolving the position of the ice bottom from the ice thermistor data to estimate the latent heat component from the growth or ablation of the bottom surface. Time averaging on monthly or greater timescales (40 to 80 days) reduces the error in the estimate to 1–2 W m^{-2}. However, single point measurements using this method have been shown to vary greatly, even contemporaneously on a single ice floe [Wettlaufer, 1991]. For the IOEB ice thermistor data, a combination of visually selected points and parametric fits of the profiles were intersected with the seawater freezing temperature to estimate the bottom to within 1–2 cm. The newer mass

balance buoys have acoustic sensors that determine the ice bottom to 1 cm with greater accuracy.

4. Results

4.1. Observations

[20] The hydrographic data from the platforms listed in Table 1 are used to calculate seawater σ and ΔT_f from each measurement from the instrument located at either 8 or 10 m in the case of buoys, or from averages between 8 and 12 m in the case of STD or CTD profiles. The values determined from the higher resolution buoy data and SHEBA yo-yo CTD are subsequently averaged on a daily basis, while the semidaily profiles from the other ice camps are not averaged. Ice drift velocities are calculated from the raw locations, and $u*$ is determined from each velocity and subsequently averaged in the same increments as the density and ΔT_f. F_w is calculated from σ, ΔT_f, and $u*$ using equation (3). Consequently, a total of 7661 points results from the observations. Some broad features of the time series stand out when the computed daily or semidaily observations from all platforms are plotted on the same axes.

[21] The annual variations of density (not shown) are obscured by the geographical variations (the surface waters in the Canada Basins are fresher). As the temperature is close to freezing, σ is controlled mostly by the salinity, so temporal changes in σ presumably reflect the infusion of brine or freshwater due to the growth or ablation of the overlying sea ice and the influence of river input.

[22] There is a clear annual cycle in the ΔT_f data, which increases in May, attains a peak around the end of July ($\sim$day 210) and decreases rapidly thereafter, and appears to vary relatively uniformly throughout the Arctic basins (Figure 2a). Between November and May, ΔT_f is generally less than 0.03°C, except for a few instances. Specifically, the enhanced ΔT_f evident just before day 300 are from a SALARGOS buoy deployed during CEAREX, and resulted from the upwelling and entrainment of entering Atlantic Water after a passing storm [Steele and Morison, 1993]. Similarly, the anomalies after day 300 are from IOEB data, and these have also been attributed to the entrainment of warmer subhalocline water due to synoptic events [Yang et al., 2001].

[23] On the other hand, there is no clear annual cycle in the $u*$ data (Figure 2b). As indicated previously, the calculations of $u*$ from ice velocity depend on the roughness of the sea ice and the upper ocean geostrophic velocity, and neglecting variations of these terms could be responsible for some error. Overall, there is a much larger amount of synoptic variability in $u*$, than in either density or ΔT_f.

[24] In Figure 2c, the annual cycle of F_w computed from all observations of σ, ΔT_f, and $u*$ closely resembles the annual cycle of ΔT_f in Figure 2a, with greater variability induced by $u*$. In Figure 3, the time series of F_w determined from each individual platform are presented, grouped according to region. The individual time series can be misleading by themselves when the geographic variations are not taken into account. The spatial distribution of F_w during the extreme winter and summer months are presented in 10-day averages from each individual platform in Figure 4. Because of the platform drifts, only in a very few areas do the data from different platforms overlap in the
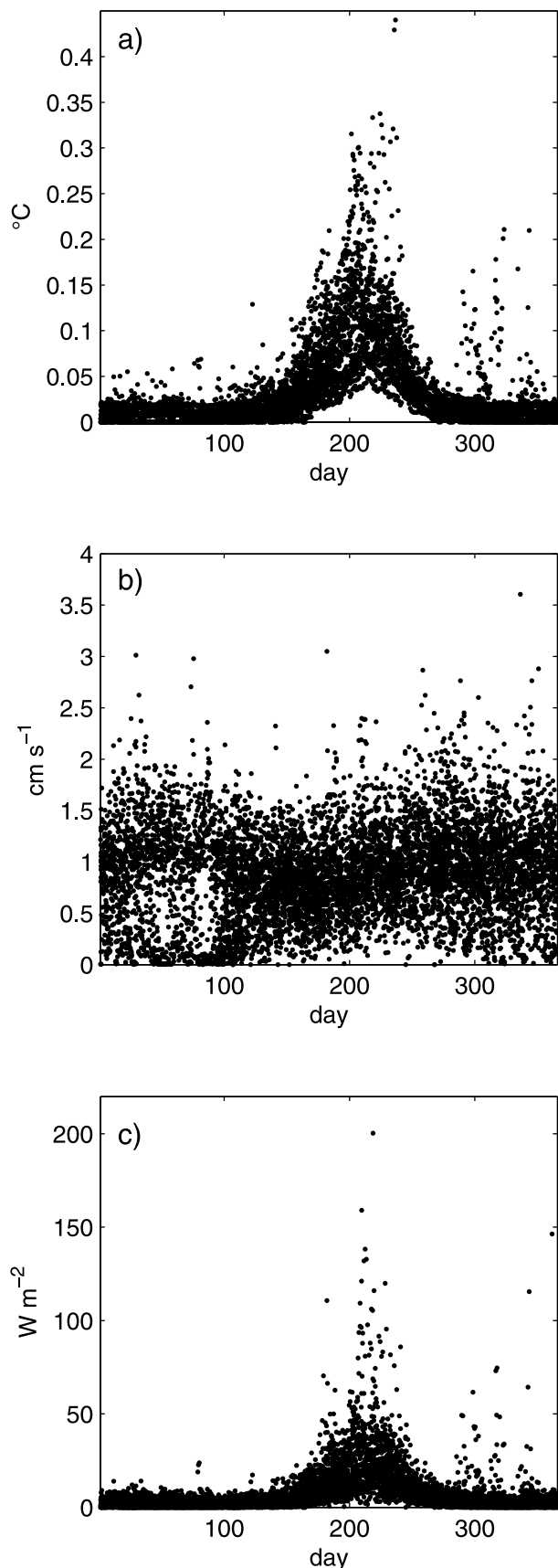
Figure 2. Daily or semidaily averages of (a) ΔT_f, (b) u^*, and (c) F_w as a function of day of year from all observations.

same region during the same time of the year, and those only do so for short periods of time. These differences in the data set make it difficult to determine the complete large-scale spatial structure and detailed temporal variability of F_w from the observations alone.

4.2. Annual Variability From Observations

[25] In a previous study, *Maykut and McPhee* [1995] used the same methods on the daily CTD data from the 5 AIDJEX camps in the Beaufort Sea in 1975–1976 to estimate F_w and found maximum values reached 40 to 60 W m^{-2} in August, for an annual average value of 5.1 W m^{-2} (where they assumed zero heat flux in winter). This compares with the calculations in the present study, where annual average F_w at AIDJEX varies depending on ice camp from 4 to 9 W m^{-2} (and no zero assumption).

[26] However, when annual estimates are determined directly from different groupings of platform time series, the results vary somewhat because of variations in time and space. Annual F_w is 7.1 W m^{-2} from all 10 platforms with observations through the summer in the Beaufort Gyre, however, when the data from one odd SALARGOS platform are removed, the annual mean is 6.6 W m^{-2}. For comparison, *Perovich and Elder* [2002] report annual average F_w at SHEBA from ice temperature profiles from four different ice types, ranging from 7.5 W m^{-2} for multiyear ice to 12.4 W m^{-2} for an old ridge. In our calculations, SHEBA F_w from ice drift and hydrographic data averages 8.4 W m^{-2}. Maximum F_w (19 W m^{-2}) was observed by two SALARGOS buoys in 1985 and 1988. Minimum annual F_w (2 W m^{-2}) was detected by the IOEB in 1996. In the Transpolar Drift, the locations of the platforms are farther north than in the Beaufort Gyre. However, as the platforms approach Fram Strait, F_w increases considerably [e.g., *Perovich et al.*, 1989]. Overall, annual average F_w calculated from the 7 SALARGOS buoys deployed in the Transpolar Drift region between 1988 and 1992 is 6.7 W m^{-2}. Averaging F_w from all observations between 1985 and 1998 equals 6.9 W m^{-2}.

[27] Monthly statistics of the quantities determined from observations are calculated altogether and separately from the platforms in the Transpolar Drift and Beaufort Gyre regions in Figure 5. While individual daily values are only as precise as 5–6 W m^{-2}, monthly (and longer) averaging reduces the standard error of the F_w estimates to better than 1 W m^{-2}. In Table 2, annual statistics are derived from monthly statistics of the daily data. Overall, mean annual F_w from the observations is not significantly different in the Beaufort Gyre and the Transpolar Drift regions.

[28] A large part of annual variability can be related to a latitudinal dependence on the solar insolation. In the summer, the heat in the upper ocean and flux of heat are larger in the Beaufort Gyre than the Transpolar Drift. On the other hand, F_w is not negligible in winter, but averages less than 2 W m^{-2} in the Beaufort Gyre, and is approximately 3 W m^{-2} in the Transpolar Drift. Because of the large seasonality of the signal, variance is large and exceeds the magnitude of the mean.

4.3. ΔT_f Parameterization

[29] Annual average ΔT_f from the observations varies from 0.03 to 0.08°C and is the most significant component
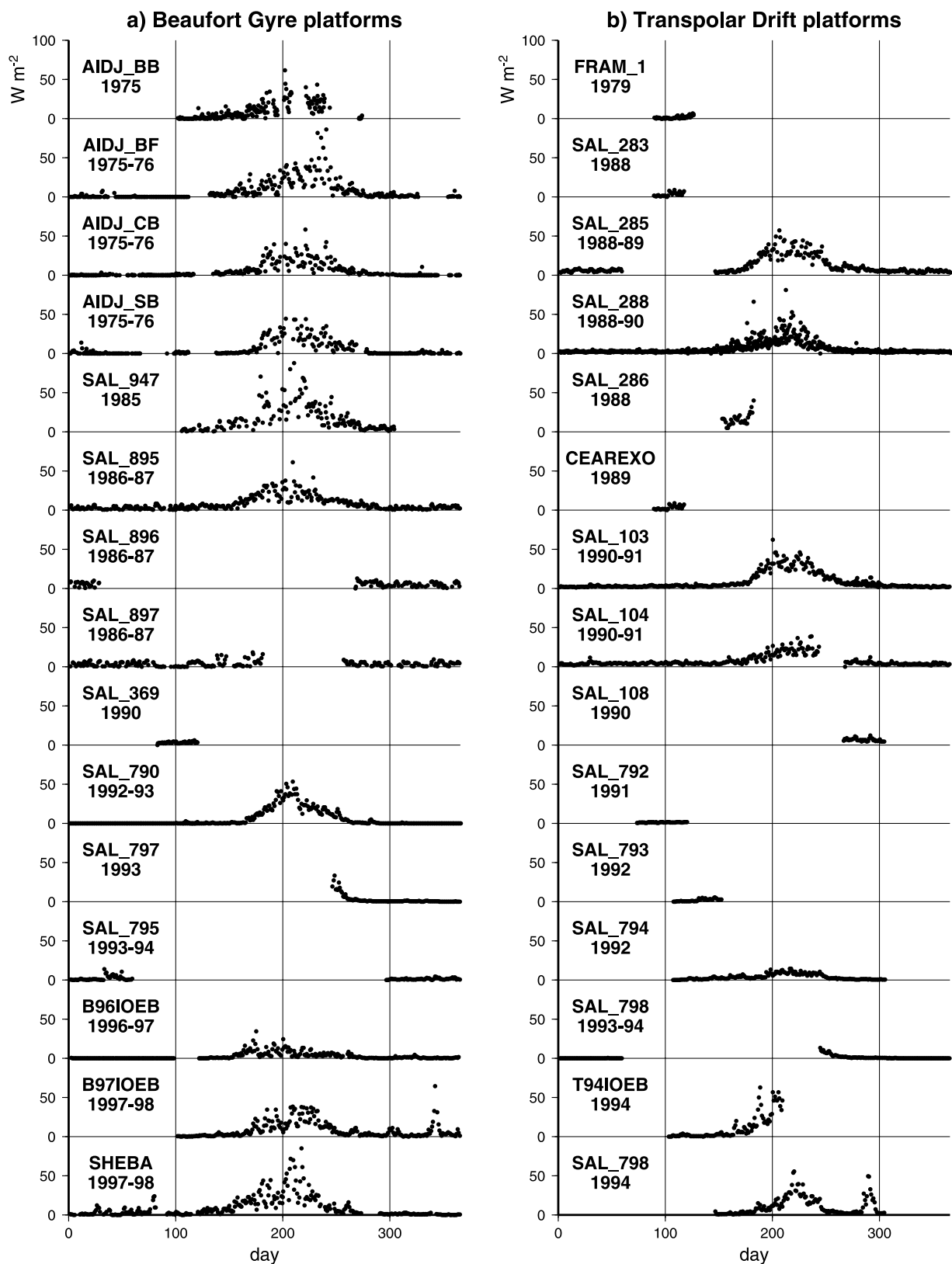
Figure 3. Daily or semidaily average time series of F_w for each individual platform in (a) Beaufort Gyre, (b) Transpolar Drift, and (c) other regions.
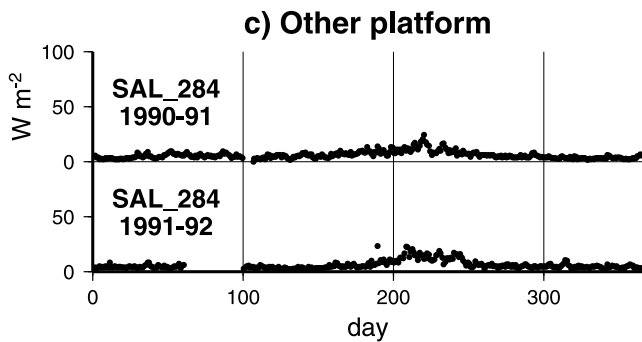
c) Other platform

Figure 3. (continued)

of the annual cycle of F_w (while σ is the least). For comparison with the observations from the drifting platforms, a climatological ΔT_f was also calculated from values of temperature and salinity at 10 m depth from the PHC. Sample plots of observed and climatological ΔT_f from several platforms with data throughout the summer period are presented in Figure 6 (along with a parameterization of ΔT_f discussed below). The differences between ΔT_f from observations versus ΔT_f from the climatology for all platforms are shown by a scatterplot in the top left plot of Figure 7 (where the Beaufort Gyre and Transpolar Drift regions are distinguished by different colors), and by a histogram in the top right plot of Figure 7. For the most part, ΔT_f from the climatology overestimates ΔT_f from the observations, and the standard deviation of the difference is $0.2°C$. Consequently, correlations between each time series from the drifting platforms and the corresponding climatological values are low (median $R^2 = 0.16$).

[30] A relatively simple statistical relationship based on the solar zenith angle (α) reproduces the observed annual signal of ΔT_f with less error than the climatology. Out of all 33 time series from observations, only 17 which spanned most of the annual cycle were selected for parameterizing ΔT_f. Using a least squares fitting algorithm the following relationship was determined:

$$\Delta T_f = 3 \cos(\alpha(t - 33))^6 + 0.01 \qquad (4)$$

where α is determined from the latitude and time, including a 33 day time lag. A contour plot of the parameterized values of ΔT_f by day of year and latitude is presented in Figure 8.

[31] ΔT_f from the observations sometimes exceeds the parameterized ΔT_f even in winter, but on average the parameterization is about $0.01°C$ higher (as indicated by offset that is added at the end of equation (4)). From the examples in Figure 6 and the second row of plots in Figure 7, it is apparent that the parameterized ΔT_f are a better fit to the ΔT_f from observations, such that the standard deviation of the differences is less than $0.03°C$. In fact, nearly 80% of the differences are less than $0.01°C$ (which produces differences in daily estimates of F_w of less than 2.5 W m^{-2} for typical $u*$ up to 1 cm s^{-1}). Furthermore, correlations between time series of ΔT_f from the observations and time series reconstructed from the parameterization are correspondingly high (median $R^2 = 0.75$). However,

it is also apparent from Figure 7 that the parameterization often overestimates the observed ΔT_f in the Beaufort Gyre, but underestimates ΔT_f in the Transpolar Drift. The parameterized ΔT_f from the locations and times of the Transpolar Drift platforms are mostly less than the observed ΔT_f by $0.01–0.02°C$, and the variability between time series is less. During summer, the regional differences between the observed and parameterized ΔT_f could be related to changes in ice concentration. However, the elevation of heat above freezing in winter is probably due to advection of heat horizontally or vertically from the subsurface Atlantic or Pacific layers.

4.4. F_w Reconstruction

[32] The high correlation of the parameterized ΔT_f to the observations suggests that incident solar radiation may be the primary source of the heat in the mixed layer beneath the pack ice. The observations were all obtained where mean annual ice concentrations were greater than 90%, so the results do not apply outside of the central pack. Furthermore, it is assumed that these results are representative to the basins, away from shelf processes and boundary currents. Consequently, the broad Eurasian shelf seas are not included in the study region.

[33] Daily parameterized ΔT_f are modulated with daily ice drift vectors for the years 1979 through 2002 from the *Fowler* [2003] data set to produce a time and space varying reconstruction of F_w throughout the Arctic, again using equation (3). Similar to the time series calculations, the geostrophic flow is not removed from the ice drift. Temperature and salinity data at 10 m from the monthly PHC climatology are converted to grids corresponding to the ice motion and interpolated in time to estimate σ, while c_p and c_h are the same constants used in the time series calculations. Since all of the seawater properties are described by a fixed annual cycle or fixed value, the interannual variations in the resulting F_w reconstruction are due solely to the ice motion dynamics.

[34] Values of $u*$ computed from the ice motion data set were consistently less than the observations (third row of plots in Figure 7). A least squares regression determined that the difference from the observations is minimized by scaling the square root of $u*$ derived from the ice vectors by a factor of 1.3 (bottom plots of Figure 7).

[35] Three-day mean ice concentration data from a combined SMMR and SSM/I data set based on the Bootstrap method [*Comiso*, 1999] were obtained from the NSIDC (available at http://www.nsidc.colorado.edu/data/nsidc-0079.html) and used to remove grid cells that contained less than 50% sea ice, and monthly and annual averages for all 24 years prepared from the daily F_w reconstruction (Figure 9). Because of the relationship of ΔT_f with α, F_w increases significantly from less than 3 W m^{-2} at the North Pole to more than 10 W m^{-2} south of 75°N. A similar pattern is reflected in the plot of the standard deviation, which largely reflects the annual cycle of parameterized ΔT_f. Because the basins and ice pack in the Beaufort Sea extend farther south than the remainder of the Arctic, F_w in this region are higher, and variations in the annual means from all areas largely reflect the variations in the southern Beaufort Sea. In the Transpolar Drift, which is farther north, the magnitude and variability of annual average F_w is less.
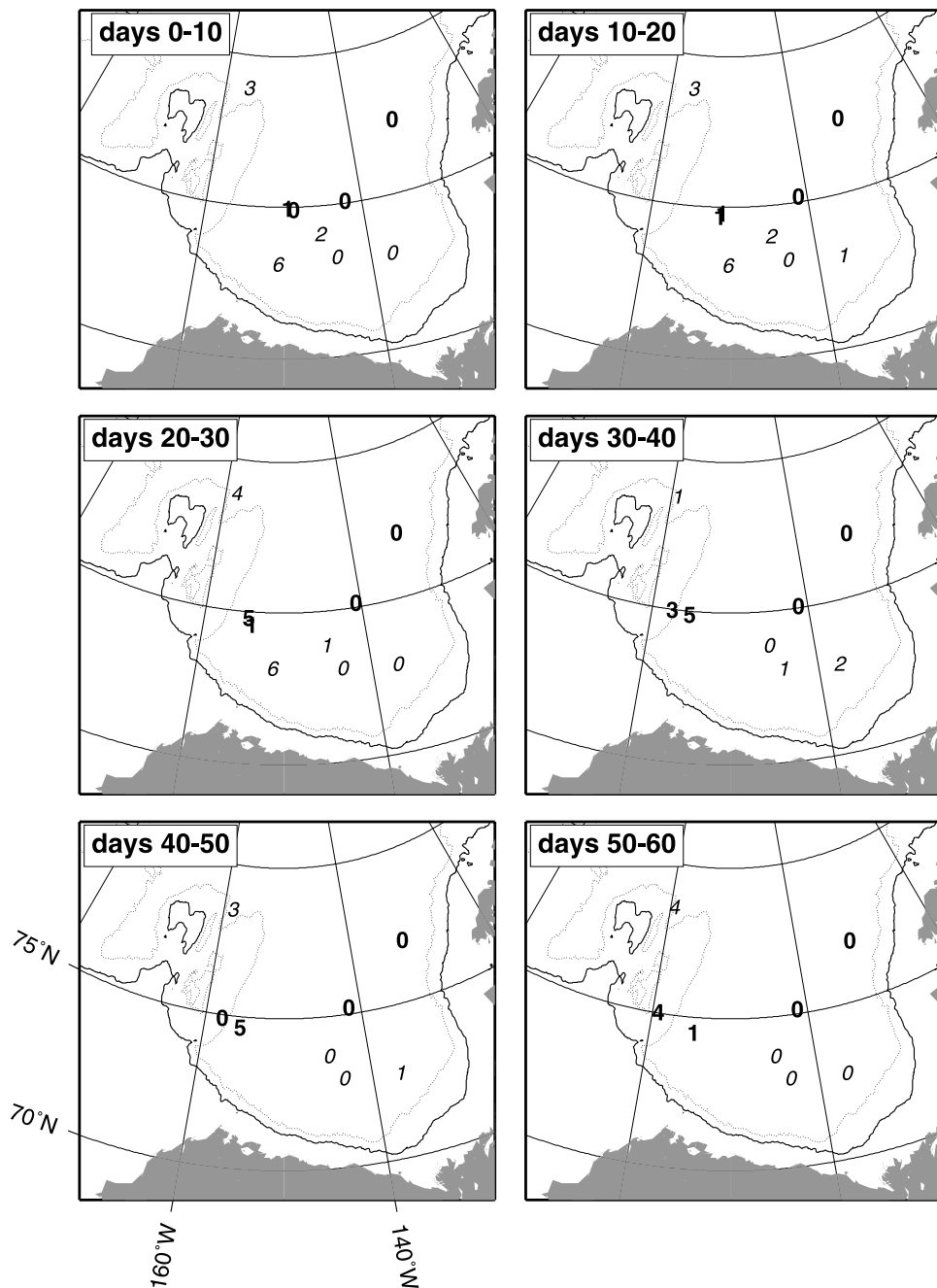
Figure 4a. Winter 10-day averages of F_w from observations in the Beaufort Gyre region plotted at platform mean locations. Italicized numbers are from observations before 1992, and bold numbers are from observations since 1992. Solid and dotted lines indicate 500 and 2000 m depth contours, respectively.
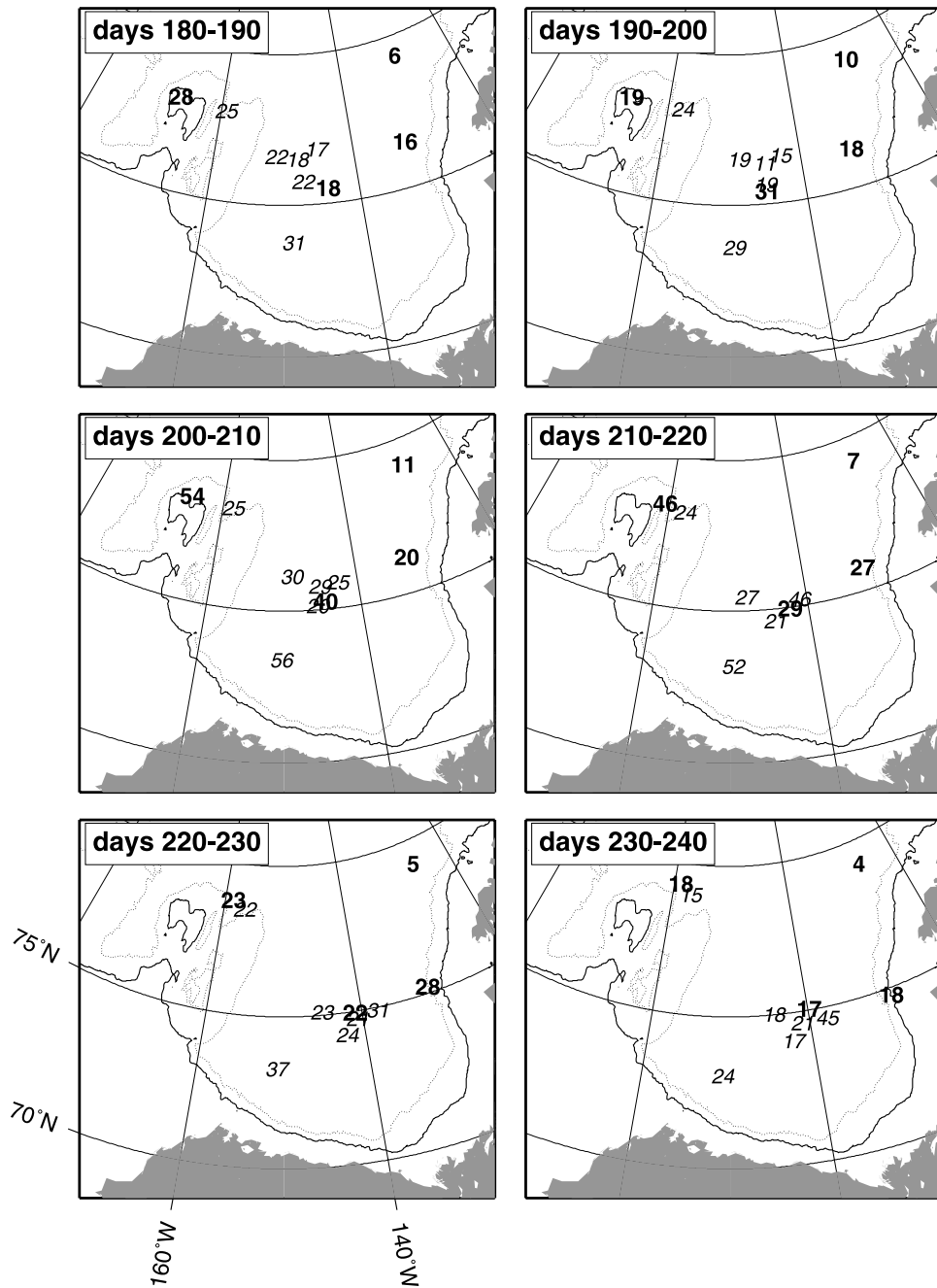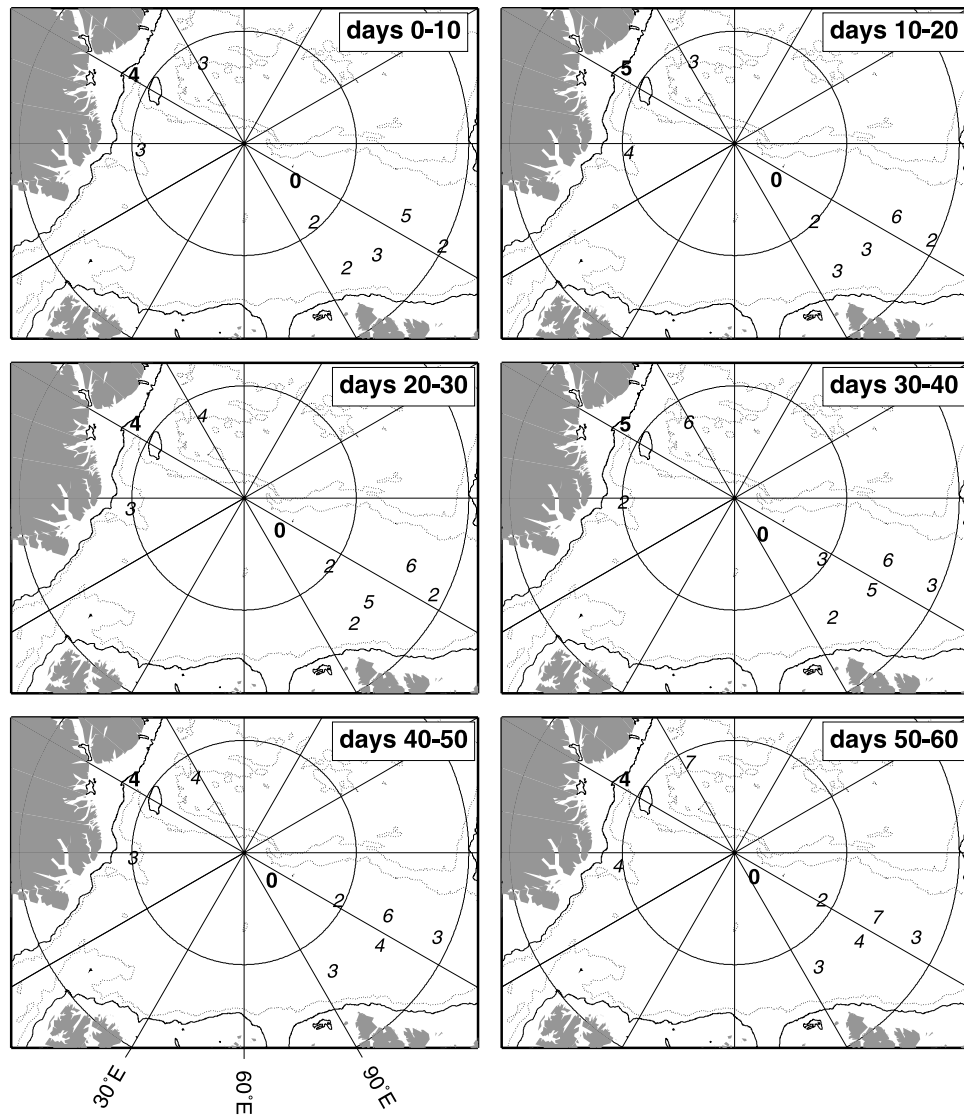
Figure 4b. Summer 10-day averages of F_w from observations in the Beaufort Gyre region plotted at platform mean locations. Italicized numbers are from observations before 1992, and bold numbers are from observations since 1992. Solid and dotted lines indicate 500 and 2000 m depth contours, respectively.
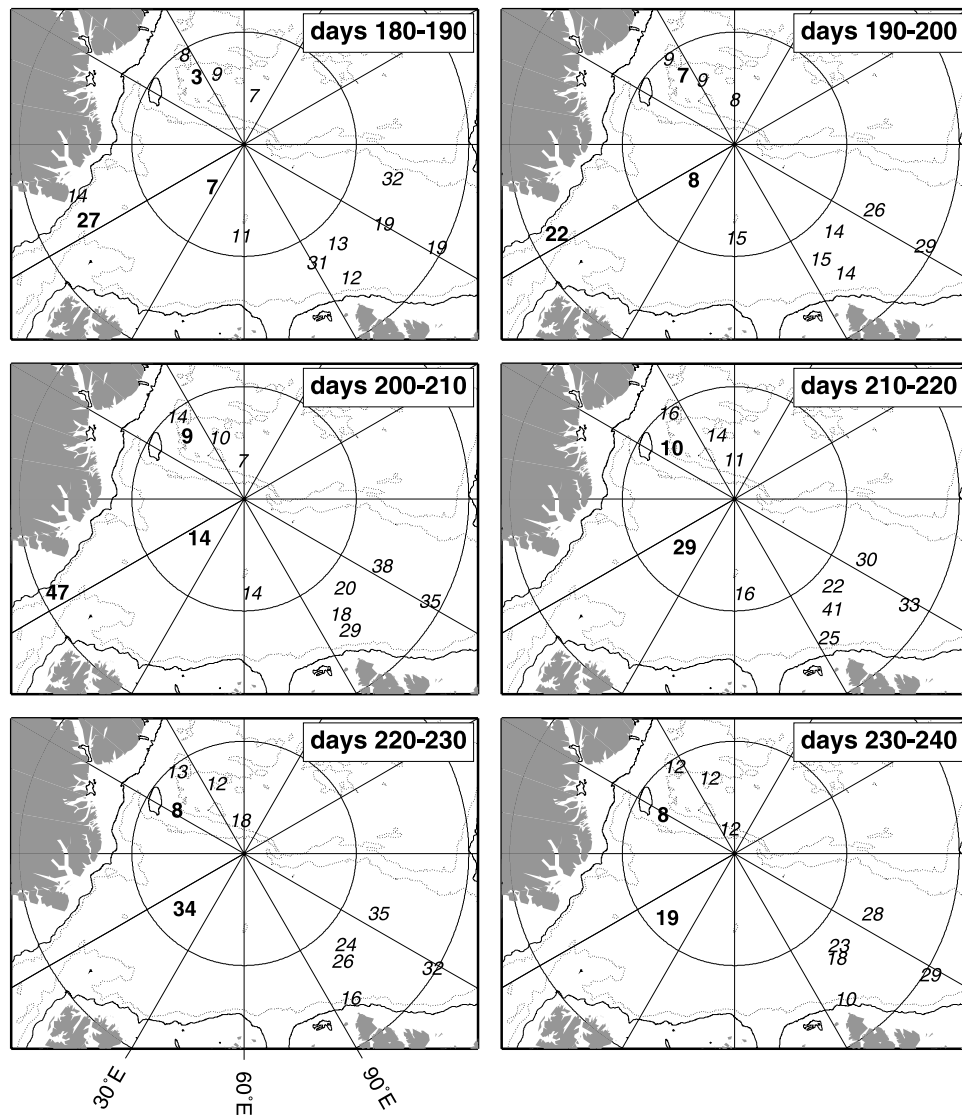
Figure 4c. Winter 10-day averages of F_w from observations in the Transpolar Drift and other regions plotted at platform mean locations. Italicized numbers are from observations before 1992, and bold numbers are from observations since 1992. Solid and dotted lines indicate 500 and 2000 m depth contours, respectively.
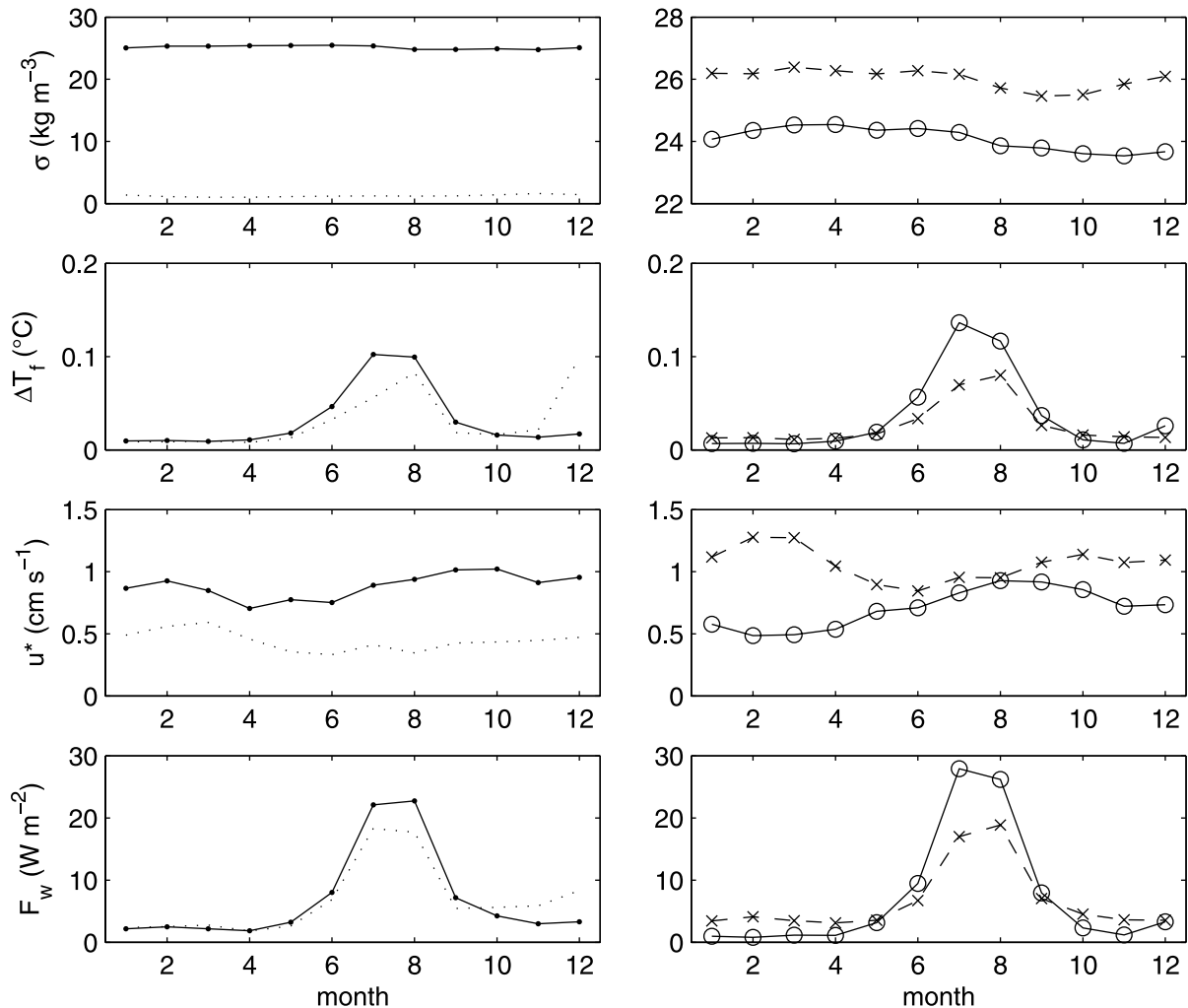
Figure 4d. Summer 10-day averages of F_w from observations in the Transpolar Drift and other regions plotted at platform mean locations. Italicized numbers are from observations before 1992, and bold numbers are from observations since 1992. Solid and dotted lines indicate 500 and 2000 m depth contours, respectively.

Figure 5. (left) Monthly means (solid lines) and standard deviations (dotted lines) of σ, ΔT_f, u^*, and F_w from all platforms. (right) Monthly means from platforms in the Beaufort Gyre (circles) and Transpolar Drift (crosses).

[36] Correlations of F_w from the parameterized reconstruction with F_w derived from the observations are moderate (median $R^2 = 0.52$). On average, the magnitudes of the mean annual and deviation determined from the observations exceed the magnitudes determined from the reconstruction at the same times and locations by 2–3 W m^{-2} (Table 2). Comparison of the observations with the reconstruction indicates that F_w in the Beaufort Gyre is enhanced compared to the Transpolar Drift, where F_w from the parameterization is less than the observations, primarily due to elevated ΔT_f observations in winter.

4.5. Residual Correction

[37] The residuals that result from the difference of the ΔT_f parameterization from observations include measurement errors, parameterization errors, and all effects that influence the mixed layer heat other than the solar angle, such as cloud properties, sea ice concentration, albedo, and internal ocean variability. Monthly averages of the residuals of F_w in the Beaufort Gyre and Transpolar Drift regions are plotted in Figure 10, and annual averages are also presented in Table 2. F_w from observations are less than reconstructed in the Beaufort Gyre, but more in the Transpolar Drift, and

the differences in the Transpolar Drift appear to lag the differences in the Beaufort Gyre.

[38] Summer F_w from observations in the Beaufort Gyre are typically less than F_w from the reconstruction. On the other hand, in the winter Transpolar Drift data, there is a constant positive difference of F_w from observations versus the reconstruction which is probably a component of heat mixed from below or advected from the perimeter. Consequently, mean annual F_w is overestimated by 1.2 W m^{-2} in the Beaufort Gyre region and underestimated by 3.1 W m^{-2} in the Transpolar Drift (Table 2). Differences of these magnitudes are significant, so that the estimates from the parameterized F_w reconstruction must be adjusted accordingly.

[39] Besides the solar angle, the open water fraction is also expected to influence F_w significantly. Part of the open water fraction is probably dependent on the solar angle, so part of the connection with F_w is implicitly included in the reconstruction. However, open water fraction depends on other factors besides solar angle, so could be a source of other interannual variability. In order to determine whether the residual differences could be simply correlated to the presence of the ice pack (which has large effects on the

Table 2. F_w From Observations and Reconstructions, Corrected and Adjusted

Years	BGY	TPD	ALL
Observations			
1975–1976	6.0		
1979–1986	11.9	7.5	10.4
1987–1991	3.0	7.3	7.8
1992–2001	5.7	7.1	5.4
Mean	**6.6**	**7.3**	**6.9**
std	8.5	7.0	7.5
Reconstruction			
Mean	**8.8**	**4.2**	**5.6**
std	10.4	3.4	5.7
Residuals			
Mean	**−1.8**	**3.1**	**1.4**
std	2.4	4.0	2.0
Corrected Reconstruction[a]			
1979–1986	5.1	4.3	4.2
1987–1991	4.9	5.0	4.5
199–2001	5.7	5.1	4.8
2002	4.3	4.4	3.9
Mean	**5.3**	**4.8**	**4.5**
std	6.7	3.7	4.9
Roughness Adjusted			
$z_0 = 0.03$ m	4.4	4.0	3.8
$z_0 = 0.01$ m	**3.9**	**3.5**	**3.3**
$z_0 = 0.005$ m	3.6	3.3	3.1

[a]BGY sector is between 120°W and 180° and south of 83°N; TPD sector is between 30°W and 150°W.

sensible and latent transfers of heat between the ocean and atmosphere, as well as albedo), anomalies of ice concentration from the satellite data were compared to the residuals, but no consistent patterns were evident. Only in some cases did a large ice concentration anomaly correspond to a large residual.

4.6. Corrected Reconstruction

[40] Observations provide time series of heat and velocity at various locations through the Arctic Ocean, while the parameterized reconstruction fixes the annual cycle of heat to the solar angle, and varies u^* according to an optimally interpolated atlas of ice velocities. Temporal and regional averages from observations provide the most precise information, but represent only certain times and locations. The reconstruction expands the geographic extent and frequency of the data, but varies only because of the dynamic component. To account for some of the time varying thermodynamic changes, the residual differences from the observations are merged with the reconstruction. By combining the information from both data sets, both the spatial structure and temporal variability of F_w to the Arctic pack ice are better resolved.

[41] Monthly mean F_w from the reconstruction are adjusted by adding a portion of smoothed 3-month averages of residuals separately for the Beaufort Gyre and Transpolar Drift regions (Figure 10). Simple bathymetric considerations prompted the selection of the boundaries (Figure 1). The Beaufort Gyre region (between 120°W and 180° and south of 83°N) is bounded approximately by the Northwind Ridge to the west, the Alpha Ridge to the north, and the continental shelves. The northern limit of the Transpolar

Drift sector (between 30°W and 150°W) is approximately delineated by the Lomonosov Ridge. Only one platform obtained observations between these regions (in the Lincoln Sea), and the monthly average residuals from that system were only slightly positive and relatively constant throughout the year. Therefore no correction is applied to the reconstruction in the area between the Beaufort Gyre and Transpolar Drift regions (encompassing the Mendeleyev Basin and Lincoln Sea).

[42] After merging with the residuals, the mean difference between monthly averages of F_w from observations and monthly averages of F_w from the reconstruction is 0.3 (±0.5) W m^{-2}, so that on average the corrected reconstruction may slightly underestimate the observations. For the longer timescales corresponding to the duration of the drift of individual platforms, average F_w from the corrected reconstruction are within 25% of the observed averages (at the 95% confidence level).

[43] The large-scale spatial characteristics of the corrected reconstruction of F_w are presented in Figure 11. The mean annual and standard deviation are mapped in the top panels, while mean anomalies for different multiyear periods are shown in the bottom panels. While there is still a large dependence on the relationship of ΔT_f with α in the corrected reconstruction, the variation is reduced and the pattern of F_w is less symmetric than in the uncorrected reconstruction. Similar changes are reflected in the plot of the standard deviation. Mean annual, and multiyear averages were calculated for all areas covered by the grid, and separately for the Beaufort Gyre and Transpolar Drift regions (Table 2).

4.7. Comparison of Annual F_w Estimates With Ice Mass Balance Measurements

[44] So far, annual estimates of the magnitude of F_w for different regions and times have been computed from the observations and the parameterized reconstruction. Because the distribution of the observations in space and time is sparse, the reconstruction was used to extrapolate these estimates throughout the whole Arctic Ocean. A portion of the residuals determined from differences from the observations fine-tunes the reconstruction in separate Arctic regions. From the corrected reconstruction the annual average F_w throughout the extent of the multiyear ice pack is estimated to be 4.5 W m^{-2}. To validate the accuracy of this estimate, these results are compared with concurrent determinations of F_w from ice thermistor profiles (Table 3) and other published results. Furthermore, the effect of the roughness parameter on the accuracy of the estimate is considered.

[45] Ice thermistor strings provide data for estimating the conductive, latent and specific heat fluxes to the bottom of the ice floe, which are combined so that F_w results. The latent and specific heat associated with ice growth and ablation are the most critical components of the equation, so that errors in measuring the position of the ice bottom are significant. Averaging time periods of a month or more reduces the error of the estimate to better than 1 W m^{-2}, but also reduces the frequency of the observations. *Maykut and McPhee* [1995] report 3.5 W m^{-2} from ice mass balance measurements in AIDJEX, and noted that estimates using hydrographic measurements were 50% greater (5.1 W m^{-2}).
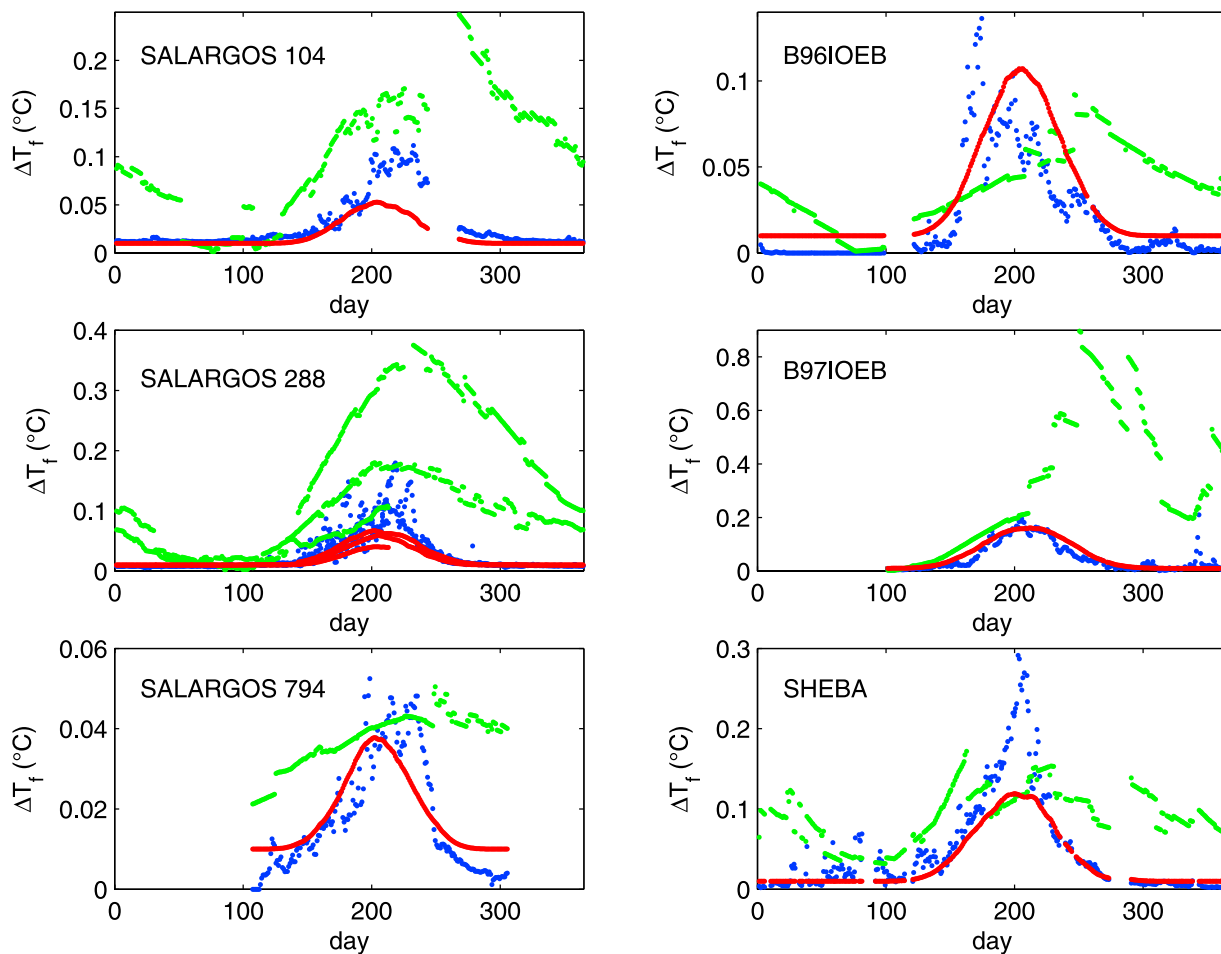
Figure 6. Annual cycle of ΔT_f at selected stations from observations (blue), climatology (green), and parameterization (red). (left) Platforms from the Transpolar Drift region and (right) platforms from the Beaufort Gyre. Note that the vertical scales are different for each platform.

Here, an independent means of estimating F_w from mass balance measurements of sea ice is provided by several automated platforms in the 1990s and early 2000s (Table 3). Most indicate mean annual averages between 2 and 4 W m^{-2} (only the SHEBA experiment provided an annual average of 8 W m^{-2}). Four of the platforms are in the Beaufort Gyre, and two of the platforms were J-CADs deployed in the Transpolar Drift as part of the North Pole Environmental Observatory [*Morison et al.*, 2002; *McPhee et al.*, 2003].

[46] Data from the SIMI ice camp in the Beaufort Sea in 1993–1994 [*Perovich et al.*, 1997] furnish an annual average F_w of 4 W m^{-2}, ranging from zero in the winter, to 5 W m^{-2} in the spring and fall, and a maximum of 9 W m^{-2} averaged through the summer. Ice thermistor data from an IOEB circulating in thick ice in the Beaufort Gyre in 1996 and 1997 average between 2 and 3 W m^{-2}. The region that the IOEB occupied in 1996 in the northeast Canadian Basin was an area of heavy ice conditions and consequently less open water, which may explain the low F_w (2.2 W m^{-2}) in 1996. Maximum ΔT_f was only about 0.10°C, and peaks of F_w were only 10–15 W m^{-2}. The following year, F_w from the hydrographic data is several W m^{-2} larger than F_w from the ice data, while during the

SHEBA year very high F_w prevailed [*Perovich and Elder*, 2002]. Thick multiyear ice floes averaged 7.5–8 W m^{-2}, ponded ice averaged 10 W m^{-2}, and ridged ice 12 W m^{-2}. In the Transpolar Drift in 2000 and 2002, ice mass balance data from the North Pole Environmental Observatory average 3 W m^{-2} while simultaneous hydrographic observations from J-CAD buoys indicate mean annual F_w between 5 and 6.5 W m^{-2} (in the study by *McPhee et al.* [2003], the same data from the 2002 system yield mean annual F_w equal to 2.6 W m^{-2} using reduced roughness length, and assuming zero F_w in winter). In general, in the late 1990s and early 2000s, F_w averages from the ice mass balance method appear to be less than averages from the hydrographic measurements by about one third (33%).

[47] Previously reported measurements of F_w in the multiyear ice pack for short time periods were made from Fram 1979 [*McPhee and Untersteiner*, 1982] where F_w was less than 2 W m^{-2} during spring, and on automated buoys during and after CEAREX [*Perovich et al.*, 1989; *Steele and Morison*, 1993] which show elevated fluxes near the perimeters where the ice pack exits the Arctic. Results from several ice thermistor sites distributed throughout a single ice floe during CEAREX by *Wettlaufer* [1991] show large variability (between 0 and 37 W m^{-2}) in spatial scales of
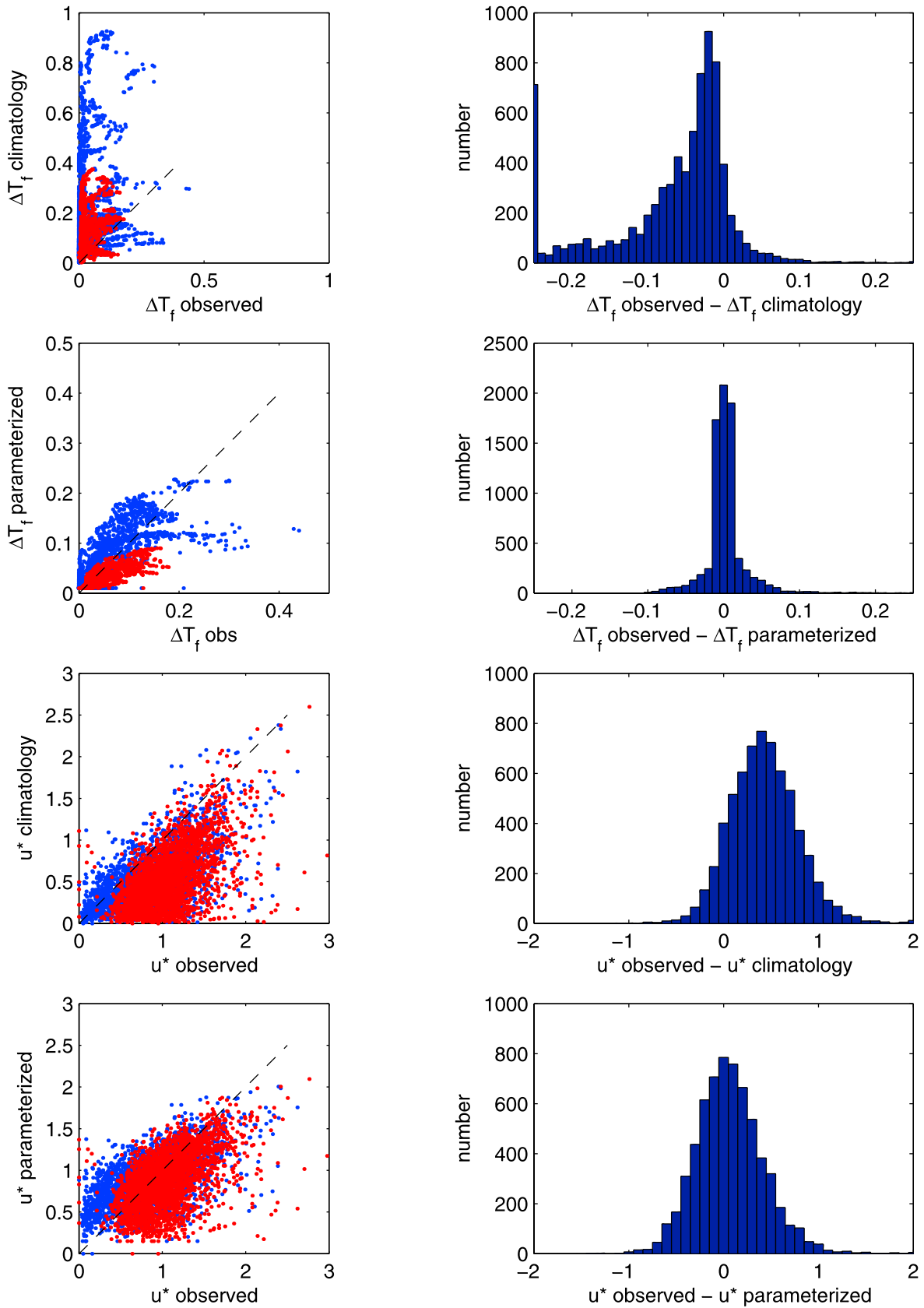
Figure 7. (left) Scatterplots of ΔT_f and $u*$ from observations versus the corresponding values from climatologies and parameterizations. Data from the Beaufort Gyre are blue, and data from Transpolar Drift are red. (right) Histograms of differences between ΔT_f and $u*$ from observations and climatologies and parameterizations.
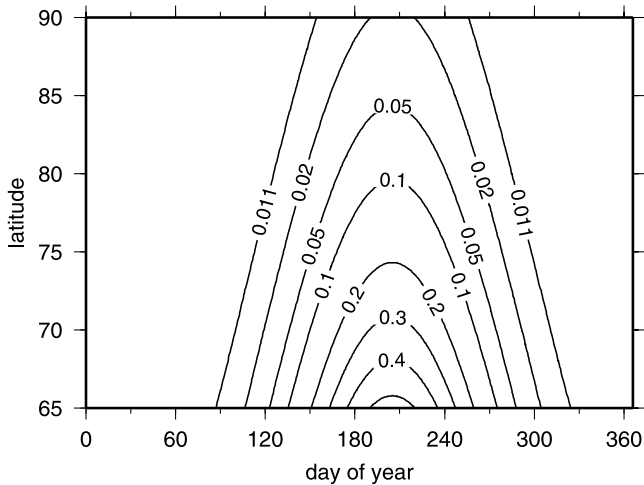
Figure 8. Parameterized ΔT_f (°C) as a function of α, by day of year and latitude.

Figure 10. Monthly differences (residuals) of observed minus reconstructed F_w (W m^{-2}), in the Beaufort Gyre (circles) and Transpolar Drift (crosses) regions. Solid and dashed lines equal one half of the 3-month average for the respective regions and indicate the monthly correction that is applied to the reconstruction for each region.

only 10–100 m during autumn. This variability can be explained in the planetary boundary layer model by changes in roughness (z_0) across the bottom topography of the ice floes that are related to the turbulent exchange at the ice-ocean interface [*McPhee*, 1992]. The present parameterization from hydrographic measurements uses a roughness length $z_0 = 0.1$ m derived during AIDJEX, but recent evidence suggests that z_0 may be as small as 0.005 m (for the smooth ice during SHEBA; *McPhee* [2002]), so $z_0 = 0.01$ m has been suggested as more representative of mean ice conditions [*McPhee et al.*, 2003]. Lowering z_0 to 0.01 m reduces F_w calculated from the hydrography by 27%, and lowering to 0.005 m by 32% (Table 2).

[48] Therefore F_w from hydrographic observations compare favorably to F_w from ice mass balance measurements when z_0 is between 0.005 and 0.01 m. Considering that the ice mass balance method may miss peaks in F_w, the best average F_w in the Arctic is probably conservatively
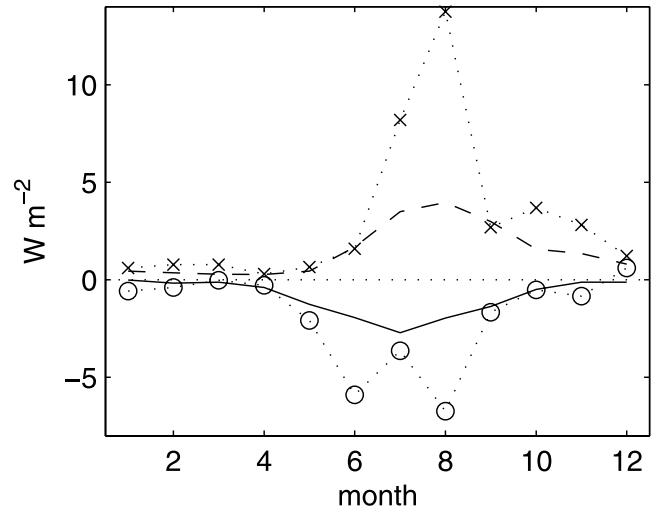
described from hydrographic measurements when z_0 equals 0.01 m. Applying this adjustment to the 4.5 W m^{-2} estimate from the corrected reconstruction yields a basin-wide average of 3.3 W m^{-2} (Table 2).

4.8. Multiannual and Interannual Variability

[49] Multiyear average F_w anomalies from the reconstruction reflect only the contribution due to variations of the ice motion. Prior to 1987, the 8-year average of F_w anomalies due to the ice drift are below the climatogical mean by several tenths W m^{-2} throughout the Arctic (Figure 11). Between 1987 and 1991, F_w anomalies in the Canadian Basins remain below the mean, but are elevated above the
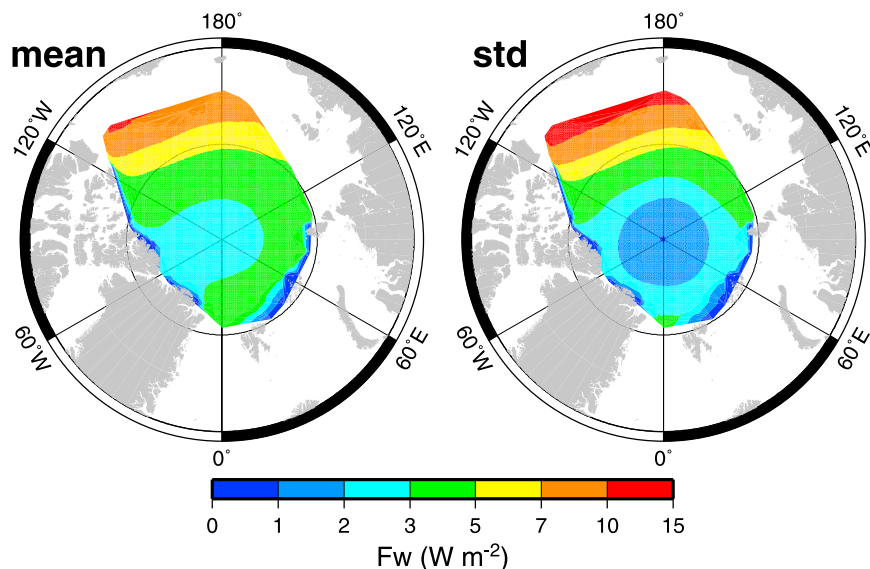

Figure 9. Annual means and standard deviations of F_w (W m^{-2}) using parameterized ΔT_f estimates and u^* from daily ice motions.
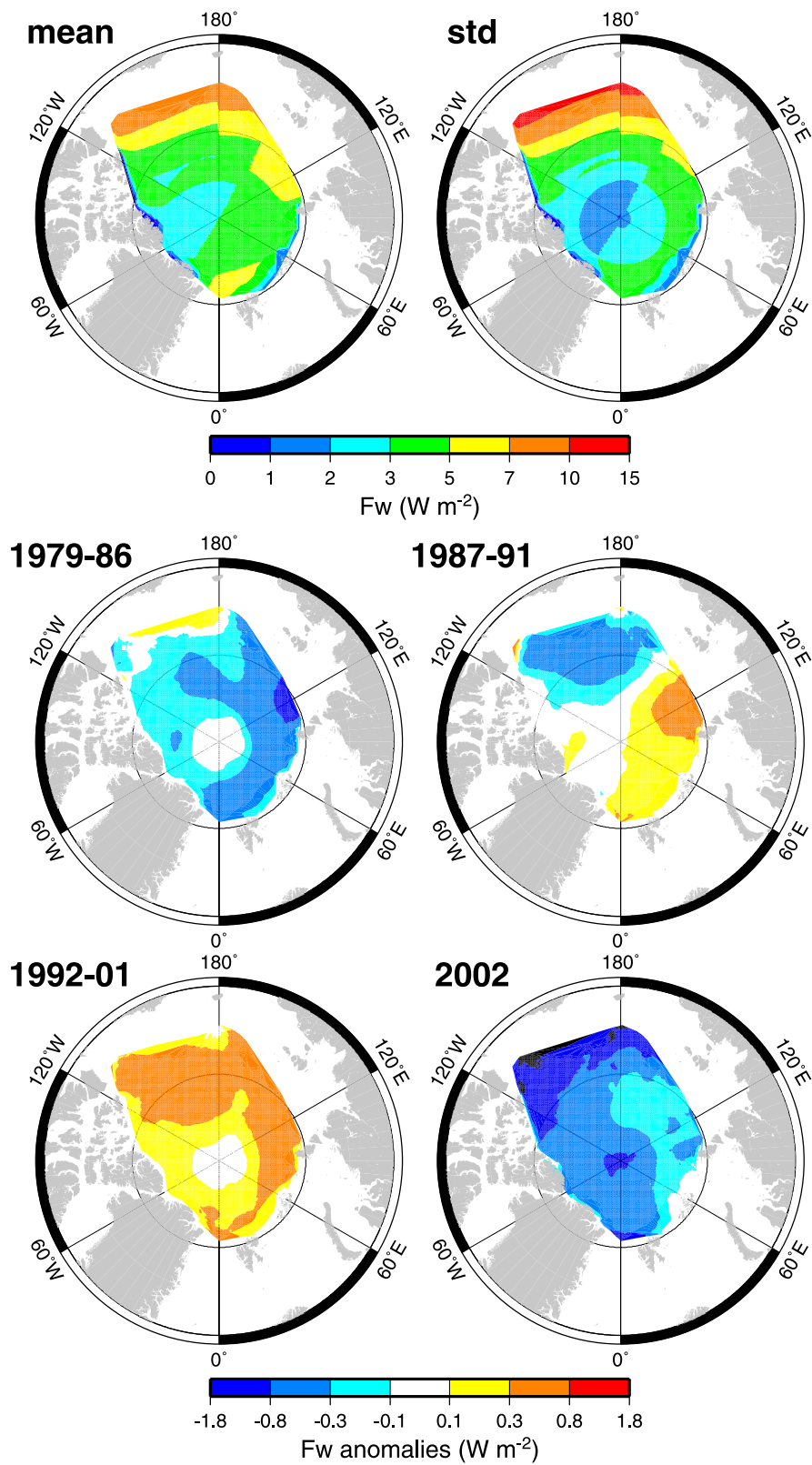
Figure 11. Annual means and standard deviation of reconstructed F_w (W m^{-2}) using parameterized ΔT_f estimates (corrected) and $u*$ from daily ice motions. The mean anomalies for four different multiyear periods are shown in the bottom plots.

Table 3. Comparison of Coincident F_w Estimates From Ice Thermistors (F_i), Mixed Layer Observations (F_w), and Corrected Reconstruction (F_{pc})

Years	Days	F_i	F_w	F_{pc}
Beaufort Gyre				
SIMI 1994	250	4.4		9.4
IOEB 1996–1997	324	2.2	2.4	4.5
IOEB 1997–1998	237	3.0	6.1	6.6
SHEBA 1997–1998	323	8.4	8.4	6.8
Transpolar Drift				
NP 2000–2001	273	3.0	6.5[a]	4.3
NP 2001–2002	237	3.0	5.2[a]	3.1

[a]CTD depth adjusted from 25 m to 10 m.

mean by about the same amount in the Eurasian Basins. After 1991 through 2001, F_w anomalies due to the ice motion exceed the climatological mean throughout the Arctic. Reduced ice motion in 2002 indicates a return to lower than average F_w everywhere, especially in the southern Beaufort Sea.

[50] The temporal variability is illustrated more clearly in Figure 12, which plots the 24-year time series of annual mean F_w for the entire Arctic from the parameterized reconstruction (corrected and adjusted for $z_0 = 0.01$ m) in the top plot, and de-meaned time series of interannual variations for selected regions in the bottom panel. Minimum average F_w occurs around 1984, and maximum in 1993, with a spread exceeding 1 W m^{-2} and an apparent trend of 0.2 W m^{-2} decade^{-1}. Interannual variability is greatest in the Beaufort Sea sector south of 75° N. There is also some indication of a step change occurring around 1990, which coincides with the well documented change of the Arctic Oscillation to a positive state [*Walsh et al.*, 1996].

[51] In the Transpolar Drift, the existence of the cold halocline is believed to isolate the Atlantic layer heat from reaching the ice pack directly. Consequently, the retreat and recovery of the halocline [*Steele and Boyd*, 1998; *Björk et al.*, 2002; *Boyd et al.*, 2002] could influence F_w particularly in the transition region over the Amundsen and Makarov Basins.

5. Discussion

[52] Observations from drifting buoys indicate that there is a significant relationship of the angle of the sun (α) with ΔT_f in the upper ocean under the Arctic ice pack. *Maykut and McPhee* [1995] suggested that most the heat of the mixed layer enters as solar radiation through leads in the ice pack rather than being diffused upward from below. Supporting a solar association, the present study indicates that most (75%) of the annual variability of F_w can be attributed to the solar angle, α. As a result, F_w from the upper ocean to the ice depends strongly on latitude. On the basis of a combination of observations, climatological data and parameterizations, annual F_w probably averages 3–4 W m^{-2} throughout the Arctic Ocean icepack.

[53] This estimate is more than the 2 W m^{-2} that was required in model simulations to equilibrate a perennial ice thickness of 3 m [*Maykut and Untersteiner*, 1971]. However, it is more consistent with other recent estimates of F_w from observations such as those by *Maykut and McPhee*

[1995], *Perovich et al.* [1997], and *McPhee et al.* [2003]. Presumably, some of the F_w in excess of 2 W m^{-2} is used to melt ice ridges (where z_0 would be larger). On the other hand, *Maykut and Untersteiner* [1971] indicate that increasing F_w from 2 to 3 W m^{-2} would decrease the equilibrium ice thickness from 3 m to about 2.1 m. Interestingly, this is exactly the same amount of ice thinning as detected by *Rothrock et al.* [2003].

[54] Since the Beaufort Gyre is located farther south than the Transpolar Drift, greater summer α means greater area average F_w, especially in the southern Beaufort Gyre. On the other hand, winter F_w that cannot be ascribed to α is 1–2 W m^{-2} in the Transpolar Drift, and is usually negligible (but not always) in the Beaufort Gyre. One explanation for winter F_w is that locally intense fluxes of heat to the surface may be entrained from below by synoptic storms [*Steele and Morison*, 1993; *Yang et al.*, 2001].

[55] The Beaufort Gyre is also where the greatest interannual variability in F_w is located, in both the observations and the reconstruction. In the reconstruction, variations in ice drift velocity in the Beaufort Gyre from the 1980s to the 1990s increase F_w by as much as 1 W m^{-2}, coincident with the positive shift of the Arctic oscillation [*Walsh et al.*, 1996]. Increased F_w in the Beaufort Sea means increased ice melt, consistent with upper ocean freshening described by *McPhee et al.* [1998]. In fact, in 1998, the circulation regime shifted from cyclonic to anticyclonic [*Proshutinsky and Johnson*, 1997], and the ice cover in the west Arctic
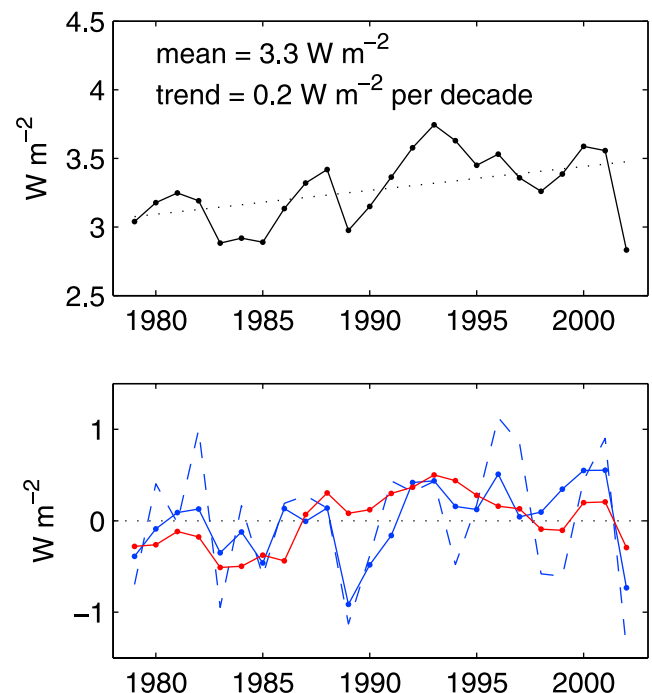

Figure 12. (top) Annual average F_w from parameterized reconstruction (corrected and adjusted for $z_0 = 0.01$ m) in all basins (solid) with trend (dotted). (bottom) De-meaned annual F_w in the Beaufort Sea sector (blue, between 120°W and 180° and south of 83°N), in the southern Beaufort Sea sector (blue dashed, between 120°W and 180° and south of 75°N), and in the Transpolar Drift sector (red, between 30°W and 150°E).

was at a minimum [*Maslanik et al.*, 1999; *Comiso et al.*, 2003]. Several years later (in 2002), our results indicate a reduction of F_w to the icepack, but at the same time as a record minimum sea ice extent was recorded throughout the entire Arctic [*Serreze et al.*, 2003].

[56] The influence of under-ice melt ponds on F_w was not addressed in this study, but recent observations and modeling [*Notz et al.*, 2003] suggest that these features could have substantial local impacts on (decreasing) the bulk heat transfer coefficient (c_h) in summer. An improved determination of large-scale F_w to the Arctic ice pack will require more year-round data from upper ocean observing platforms, and a better understanding of the spatial and temporal variabilities of ice roughness (z_0) and melt ponds (on c_h).

References

Bauer, E., K. Hunkins, T. O. Manley, and W. Tiemann (1980), Arctic Ice Dynamics Joint Experiment 1975–76, physical oceanography data report, salinity, temperature and depth data, *Tech Rep. 8-11*, vols. 1–4, pp. CU-8-80–CU-11-80, Lamont-Doherty Earth Obs., Columbia Univ., Palisades, New York.

Björk, G., J. Söderkvist, P. Winsor, A. Nikolopoulos, and M. Steele (2002), Return of the cold halocline layer to the Amundsen basin of the Arctic Ocean: Implications for the sea ice mass balance, *Geophys. Res. Lett.*, 29(11), 1513, doi:10.1029/2001GL014157.

Boyd, T. J., M. Steele, R. D. Muench, and J. T. Gunn (2002), Partial recovery of the Arctic Ocean halocline, *Geophys. Res. Lett.*, 29(14), 1657, doi:10.1029/2001GL014047.

Comiso, J. (1999), Bootstrap sea ice concentrations for NIMBUS-7 SMMR and DMSP SSM/I, http://nsidc.org/data/nsidc-0079.html, Natl. Snow and Ice Data Cent., Boulder, Colo.

Comiso, J. C. (2002), A rapidly declining perennial sea ice cover in the Arctic, *Geophys. Res. Lett.*, 29(20), 1956, doi:10.1029/2002GL015650.

Comiso, J. C., J. Yang, S. Honjo, and R. Krishfield (2003), Detection of change in the Arctic using satellite and in situ data, *J. Geophys. Res.*, 108(C12), 3384, doi:10.1029/2002JC001347.

Fofonoff, P., and R. C. Millard Jr. (1983), Algorithms for computation of fundamental properties of seawater, *UNESCO Tech. Pap. Mar. Sci.*, 44, 53 pp.

Fowler, C. (2003), Polar Pathfinder daily 25 km EASE-Grid sea ice motion vectors, http://nsidc.org/data/nsidc-0116.html, Natl. Snow and Ice Data Cent., Boulder, Colo.

Honjo, S., T. Takizawa, R. Krishfield, J. Kemp, and K. Hatakeyama (1995), Drifting buoys make discoveries about interactive processes in the Arctic Ocean, *Eos Trans. AGU*, 76, 209, 215.

Kikuchi, T., and M. Hosono (2003), *J-CAD Data Report: April 2000– March 2003* [CD-ROM], version 1.01, Jpn. Mar. Sci. and Technol. Cent., Yokosuka, Japan, Oct.

Krishfield, R., K. Doherty, and S. Honjo (1993), Ice-ocean environmental buoys (IOEB): Technology and deployment in 1991–1992, *Tech. Rep. WHOI-93-45*, 86 pp., Woods Hole Oceanogr. Inst., Woods Hole, Mass.

Krishfield, R., S. Honjo, T. Takizawa, and K. Hatakeyama (1999), IOEB archived data processing and graphical results from April 1992 through November 1998, *Tech. Rep. WHOI-99-12*, 91 pp., Woods Hole Oceanogr. Inst., Woods Hole, Mass.

Maslanik, J. A., M. C. Serreze, and T. Agnew (1999), On the record reduction in 1998 western Arctic sea-ice cover, *Geophys. Res. Lett.*, 26, 1905–1908.

Maykut, G. A. (1982), Large-scale heat exchange and ice production in the central Arctic, *J. Geophys. Res.*, 87, 7971–7984.

Maykut, G. A., and M. G. McPhee (1995), Solar heating of the Arctic mixed layer, *J. Geophys. Res.*, 100, 24,691–24,703.

Maykut, G. A., and D. K. Perovich (1987), The role of shortwave radiation in the summer decay of a sea ice cover, *J. Geophys. Res.*, 92, 7032–7044.

Maykut, G. A., and N. Untersteiner (1971), Some results from a time-dependent thermodynamic model of sea ice, *J. Geophys. Res.*, 76, 1550–1575.

McPhee, M. G. (1979), The effect of the oceanic boundary layer on the mean drift of pack ice: Application of a simple model, *J. Phys. Oceanogr.*, 9, 388–400.

McPhee, M. G. (1992), Turbulent heat flux in the upper ocean under sea ice, *J. Geophys. Res.*, 97, 5365–5379.

McPhee, M. G. (2002), Turbulent stress at the ice/ocean interface and bottom surface hydraulic roughness during the SHEBA drift, *J. Geophys. Res.*, 107(C10), 8037, doi:10.1029/2000JC000633.

McPhee, M. G., and T. P. Stanton (1996), Turbulence in the statically unstable oceanic boundary layer under Arctic leads, *J. Geophys. Res.*, 101, 6409–6428.

McPhee, M. G., and N. Untersteiner (1982), Using sea ice to measure vertical heat flux in the ocean, *J. Geophys. Res.*, 87, 2071–2074.

McPhee, M. G., T. P. Stanton, J. H. Morison, and D. G. Martinson (1998), Freshening of the upper ocean in the Arctic: Is perennial sea ice disappearing?, *Geophys. Res. Lett.*, 25, 1729–1732.

McPhee, M. G., T. Kikuchi, J. H. Morison, and T. P. Stanton (2003), Ocean-to-ice heat flux at the North Pole environmental observatory, *Geophys. Res. Lett.*, 30(24), 2274, doi:10.1029/2003GL018580.

Morison, J. H., S. P. Burke, H. Steltner, and R. Andersen (1982), SALARGOS temperature-conductivity buoys, paper presented at Oceans '82, Inst. of Electr. and Electron. Eng., Washington, D. C.

Morison, J. H., et al. (2002), Early results from the North Pole environmental observatory, *Eos Trans. AGU*, 83(33), 357.

Notz, D., M. G. McPhee, M. G. Worster, G. A. Maykut, K. H. Schlünzen, and H. Eicken (2003), Impact of underwater-ice evolution on Arctic summer sea ice, *J. Geophys. Res.*, 108(C7), 3223, doi:10.1029/2001JC001173.

Perovich, D. K., and B. Elder (2002), Estimates of ocean heat flux at SHEBA, *Geophys. Res. Lett.*, 29(9), 1344, doi:10.1029/2001GL014171.

Perovich, D. K., W. B. Tucker III, and R. A. Krishfield (1989), Oceanic heat flux in Fram Strait measured by a drifting buoy, *Geophys. Res. Lett.*, 16, 995–998.

Perovich, D. K., B. C. Elder, and J. A. Richter-Menge (1997), Observations of the annual cycle of sea ice temperature and mass balance, *Geophys. Res. Lett.*, 24, 555–558.

Perovich, D. K., T. C. Grenfell, J. A. Richter-Menge, B. Light, W. B. Tucker, and H. Eicken (2003), Thin and thinner: Ice mass balance measurements during SHEBA, *J. Geophys. Res.*, 108(C3), 8050, doi:10.1029/2001JC001079.

Proshutinsky, A. Y., and M. A. Johnson (1997), Two circulation regimes of the wind-driven Arctic Ocean, *J. Geophys. Res.*, 102, 12,493–12,514.

Rothrock, D. A., J. Zhang, and Y. Yu (2003), The Arctic ice thickness anomaly of the 1990s: A consistent view from observations and models, *J. Geophys. Res.*, 108(C3), 3083, doi:10.1029/2001JC001208.

Serreze, M. C., J. A. Maslanik, T. A. Scambos, F. Fetterer, J. Stroeve, K. Knowles, C. Fowler, S. Drobot, R. G. Barry, and T. M. Haran (2003), A record minimum arctic sea ice extent and area in 2002, *Geophys. Res. Lett.*, 30(3), 1110, doi:10.1029/2002GL016406.

Steele, M., and T. Boyd (1998), Retreat of the cold halocline layer in the Arctic Ocean, *J. Geophys. Res.*, 103, 10,419–10,435.

Steele, M., and J. H. Morison (1993), Hydrography and vertical fluxes of heat and salt northeast of Svalbaard in autumn, *J. Geophys. Res.*, 98, 10,013–10,024.

Steele, M., R. Morley, and W. Ermold (2001), PHC: A global ocean hydrography with a high-quality Arctic Ocean, *J. Clim.*, 14, 2079–2087.

Walsh, J. E., W. L. Chapman, and T. L. Shy (1996), Recent decrease of sea level pressure in the central Arctic, *J. Clim.*, 9, 480–485.

Wettlaufer, J. S. (1991), Heat flux at the ice-ocean interface, *J. Geophys. Res.*, 96, 7215–7236.

Yang, J., J. Comiso, R. Krishfield, and S. Honjo (2001), Synoptic storms and the development of the 1997 warming and freshening event in the Beaufort Sea, *Geophys. Res. Lett.*, 28, 799–802.

————————————

R. A. Krishfield, Woods Hole Oceanographic Institution, MS 23, Woods Hole, MA 02543, USA. (rkrishfield@whoi.edu)

D. K. Perovich, Cold Regions Research and Engineering Laboratory, Hanover, NH 03755, USA.